Journal of African Earth Sciences 219 (2024) 105390

Contents lists available at ScienceDirect

Journal of African Earth Sciences

journal homepage: www.elsevier.com/locate/jafrearsci

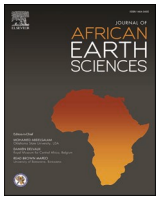

Active deformation in the central section of the East African Rift from tectonic, volcanic, and hydrologic processes: Observations from satellite geodesy

Kyle Dennis Murray [a,*], Cynthia J. Ebinger [b]

[a] University of Hawaii, Department of Earth Sciences, 2500 Campus Rd, Honolulu, 96822, Hawaii, USA
[b] Department of Earth and Environmental Sciences, 6823 St Charles Ave, New Orleans, 70118, Louisiana, USA

ARTICLE INFO

Handling Editor: M Mapeo

Keywords:
East african rift
InSAR
Radar imaging
Interferometry
Crustal deformation
GNSS
GPS
Kivu rift
Kenya rift
Mount Suswa
Nyiragongo
Olkaria
Nairobi
Groundwater subsidence
Geothermal

ABSTRACT

The East African Rift System (EARS) is an active continental rift zone that hosts a diverse range of processes that result in recent and ongoing crustal deformation. To analyze these processes, we used Sentinel-1 Interferometric Synthetic Aperture Radar (InSAR) to complement the sparse GNSS velocity field with high resolution measurements of line-of-sight (LOS) deformation between 2015 and 2022. A broad survey approach was employed to detect new signals within the central section of the EARS, and to establish a baseline for future studies focused on tectonic, volcanic, and/or hydrologic deformation and change spanning geodetic time scales. With this regional approach, we were able to resolve signals varying over time-spans of a few weeks to several years that have magnitudes greater than ~1 cm/yr. Our resulting deformation field shows a diverse range of signals related to the processes listed above as well as other unknown sources. This includes up to 8.5 cm/yr of groundwater-related subsidence in Nairobi, up to 70 cm of LOS displacement during the eruption of Nyiragongo in 2021, and steady uplift in the Manyara basin with a rate of 2.8 cm/yr. We update previously published InSAR measurements of Mount Suswa volcano, and the geothermal fields in Olkaria. We also show LOS change ranging between 2 and 5 mm/yr over a distances of approximately 200 km spanning the Kenya Rift with the greatest differential rates occurring south of Lake Turkana. More generally, our results highlight the ambiguity of relying solely on the sparse network of GNSS for studies such as those characterizing tectonic motion and rift opening. Such studies are likely missing many important signals and/or includes sites that are contaminated with signals unrelated to the target process.

1. Introduction

Crustal deformation results from a wide range of Earth processes, from tectonic forces and seismic activity, magma transport in volcanic systems, to poroelastic responses from groundwater extraction. Space-based geodetic measurements, particularly through Global Navigation Satellite Systems (GNSS) and Interferometric Synthetic Aperture Radar (InSAR), have revolutionized our ability to monitor these movements. However, while many studies have investigated broad plate motion of the EARS, our understanding of intraplate deformation remains limited in the central East African Rift System (EARS) despite the abundance and diversity of active processes there.

This study aims to address the gap in understanding how tectonic, volcanic, and anthropogenic factors contribute to the spatial and temporal distribution of strain across the central section of the EARS. By measuring the distribution of strain across and along the EARS over decadal time scales, this research seeks to elucidate the impact of lithospheric structure on deformation and magmatism, as well as the effects of anthropogenic processes that cause localized deformation, which can lead to less reliable estimates of tectonic deformation. In this paper, we detail an approach emphasizing comprehensive data management, cloud computing workflows, and data processing techniques. We present time series products that shed light on the distribution of strain in space and time, highlighting the presence of tectonic, volcanic, and anthropogenic deformation signals. Our broad survey approach enables us to identify new signals associated with a variety of processes, update time series for previously documented signals, as well as establish a baseline for climate and geophysical change.

* Corresponding author.
E-mail address: murray8@hawaii.edu (K.D. Murray).

https://doi.org/10.1016/j.jafrearsci.2024.105390
Received 24 October 2023; Received in revised form 6 August 2024; Accepted 15 August 2024
Available online 22 August 2024
1464-343X/

1.1. Tectonic setting

The EARS is a ~5000 km-long divergent boundary and is Earth's prime example of an active continental rift evolving toward an oceanic spreading center (e.g., Mcconnell, 1967). Although the EARS is attributed to the impingement of one or more mantle plumes (e.g., Boyce et al., 2023), its surface expression and presence or absence of magmatism are spatially and temporally variable in large part owing to the heterogeneity of the overlying lithosphere, which includes thick Archean cratons (e.g., Fishwick and Bastow, 2011). These heterogeneities are thought to be the main factors driving strain localization above a large-scale mantle upwelling. Yet, little is known about the decadal time scales of intraplate deformation.

The Oligocene-Recent EARS extends south of the Ethiopia-Yemen flood basalt province, consisting of two rift zones flanking the Archean Tanzania Craton (Fig. 1). Active deformation within the EARS is complex, with sparse GNSS observations suggesting a four-plate model involving the large Somalia and Nubia plates, separated by the smaller Victoria (Tanzania Craton) and Rovuma plates (e.g., Stamps et al., 2021). Challenges in understanding crustal deformation arise from the lack of GNSS data in remote areas, particularly west and north of the Western rift and offshore regions.

1.2. Hydrology

By Late Pliocene time, rift flank uplift diverted most drainage east and west, away from the Western and Eastern rift, leading to the formation of Lake Victoria between the two rift valleys (e.g., Johnson et al., 2000). The weakly magmatic Western rift has deep basins and extensive along-axis drainage, whereas the volcano-studded Eastern rift has shallower alkaline lakes in part influenced by the accommodation of strain by magma intrusion, rather than the largely-fault controlled extension in the Western rift (e.g., Ebinger and Casey, 2001). Surface water resources in East Africa are limited, with rivers in all but the highest elevation zones being seasonal and prone to flash flooding. Groundwater is an important source of water for many communities in East Africa. Overuse of groundwater resources can lead to the depletion, compaction and permanent decreased storage of aquifers, which is often accompanied by crustal subsidence (e.g., Murray and Lohman, 2018). Furthermore, widespread removal of groundwater (and surface water), can also lead to broad-scale uplift (e.g., Borsa et al., 2014).

1.3. Geodesy

Space-based geodetic measurements of crustal motion have greatly advanced our understanding of many active Earth processes in recent decades. Continuous measurements from GNSS have proven to be particularly useful for studying processes spanning large spatial scales such as tectonic motion of continents (e.g., Birhanu et al., 2016; Stamps et al., 2021). These point measurements have the benefit of high temporal sampling rates (daily or sub-daily) which provide detailed histories of deformation without temporal aliasing. Installing and maintaining GNSS stations to record ground deformation is often difficult, however, leaving many parts of the Earth with very low network density and long temporal gaps. This often leads to spatial aliasing or omissions of important deformation signals spanning areas between stations or spanning temporal gaps. Thus, the degree to which strain rates are concentrated across the EARS, particularly the central branches, remains largely unknown. Due to the network sparsity, many processes that cause deformation over shorter spatial scales (<200 km) such as fault creep, magmatic activity (e.g., volcanic deflation/inflation), and anthropogenic deformation (e.g., subsidence related to

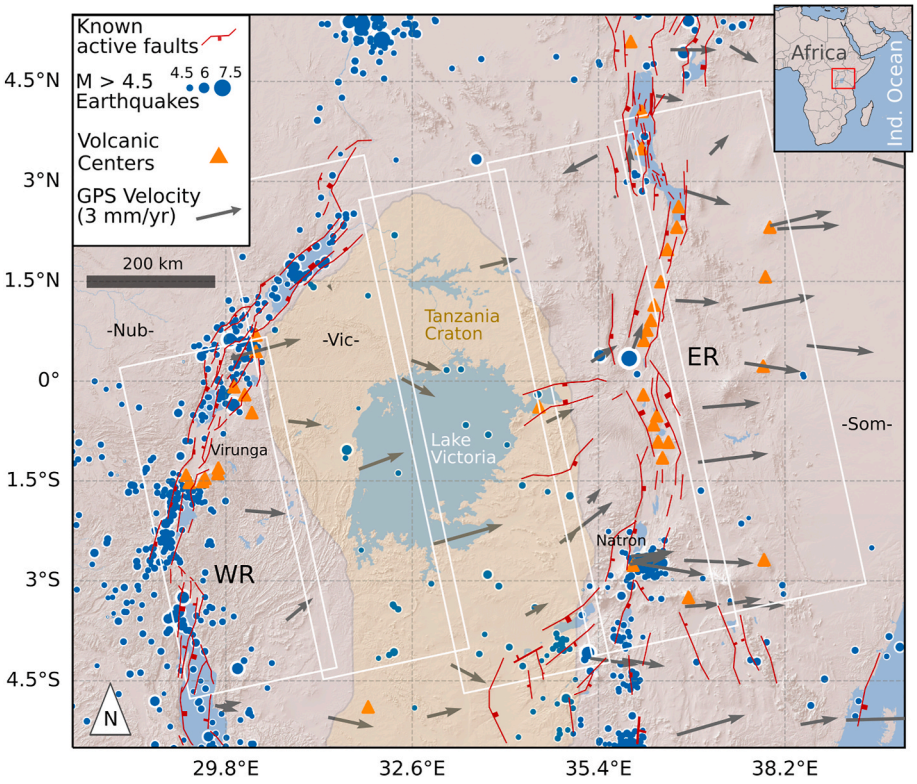

Fig. 1. Study area showing the Western rift (WR) and Eastern rift (ER) that formed around the unusually thick lithosphere of the Tanzania craton (yellow shaded region). White rectangles show locations of ascending Sentinel-1a/b paths used in this study. GNSS velocity field (vectors; King et al., 2019; Knappe et al., 2020) show general eastward velocity increase as the Nubia plate separates from the Somalia plate. Teleseismically detected earthquakes from 1976 to 2021 from NEIC (blue circles), Holocene volcanoes (orange triangles; Venzke, 2013), and faults (red lines (Ebinger et al., 2024)) are shown. GNSS sites are referenced to the stable African (Nubian) plate and span variable time ranges from 2002 to 2022. Nubian (Nub), Victorian (Vic), and Somalian (Som) plates are labeled.

groundwater extraction), are either undetected or are sampled, at most, by one or two GNSS stations, which prohibits proper characterization of the signal.

The satellite imaging technique InSAR complements GNSS measurements with measurements of crustal deformation at much higher resolution. For example, Sentinel-1 records a swath-width of approximately 250 km with a pixel spacing of approximately 3 × 22 m. InSAR allows us to fill in gaps left by GNSS and adds more spatial context to better understand the variety of source processes affecting measurements at the surface. Furthermore, it is largely unknown the degree to which shallow crustal processes, such as groundwater pore pressure changes, may impact the observed displacement signals at GNSS sites. This information is critical for planners as population growth increasingly taxes groundwater reserves. The ongoing exponential increase of freely available SAR data from the European Space Agency's (ESA) recent Sentinel-1a and -1b missions and the NASA-ISRO SAR (NISAR) mission, are enabling the production of rich time series of deformation across many parts of the Earth previously limited by low coherence and insufficient temporal coverage of SAR data. In addition, advances in data processing techniques and cloud-computing are enabling InSAR to be used across increasingly large spatial extents spanning tectonic provinces (e.g., Weiss et al., 2020). Limitations of InSAR include lower sampling rates (~weekly), single dimensionality, and noise from atmospheric conditions or changes in ground-surface properties between acquisitions (e.g., crop growth or soil moisture). Thus, combining these two modern geodetic methods (InSAR and GNSS) provides a more complete picture of crustal deformation across different temporal and spatial scales, with mostly independent noise characteristics.

Previous studies leveraging GNSS data in the EARS have primarily focused on large scale deformation trends used to characterize plate motion rates (Bendick et al., 2006; Knappe et al., 2020; Stamps et al., 2021), construction of large scale strain rate maps (e.g., Stamps et al., 2018), comparison of seismic and geodetic strain (e.g., Lavayssiere, 2019; Weinstein et al., 2017), volcano monitoring (e.g., Biggs et al., 2009; Wauthier et al., 2018) and characterization of seasonal signals (e.g., Birhanu et al., 2018). More focused studies have primarily targeted the Main Ethiopian and Afar sectors in the north where opening velocities are $\geq$ 5 mm/yr. This is an area with relatively higher station density allowing for mesoscale studies of strain variations (e.g., Bilham et al., 1999; Birhanu et al., 2016).

Similarly to GNSS-based studies, InSAR has been incorporated in previous studies to measure deformation primarily in the Afar sector of the EARS (e.g., Doubre and Peltzer, 2007; Temtime et al., 2018). Many geodetic studies of the EARS have targeted the 2005 Afar Dabbahu diking event (e.g., Wright et al., 2006; Hamling et al., 2014), and the 2007–2008 northern Tanzania rifting episode (e.g., Baer et al., 2008; Jones et al., 2019). Volcano deformation has also been measured and documented in the Western and Eastern rifts (e.g., Wauthier et al., 2009; Albino and Biggs, 2021). More recent geodetic studies have begun to measure fault-related deformation during the interseismic and co-seismic parts of the cycle in the Western and Eastern rifts using elevation models (Hodge et al., 2018) and SAR data (e.g., Zheng et al., 2020; Gaherty et al., 2019), which may provide new insights into faulting, magmatism, and hydrologic processes in rift zones. Wauthier et al. (2018) use Sentinel-1 data to delineate zones of rift basin subsidence and their relation to volcano degassing in the Virunga volcanic province, Western rift, informing regional geo-hazards.

We use both GNSS and InSAR measurements of crustal deformation to highlight strain concentrations across the central section of the EARS (Fig. 1), including areas with and without surface magmatism. In the following sections, we delve into the specifics of our methodology, data analysis, and the consequential findings that shed new light on the numerous sources of active deformation in the EARS.

2. Data and methods

2.1. GNSS data

The GNSS network covering the EARS is supported by a range of institutions and investigators. We used the velocity field computed by King et al. (2019) in combination with point position time series and velocities available from the University of Nevada Reno Geodetic Laboratory (http://geodesy.unr.edu) (Fig. 1). All GNSS data presented is referenced to the stable African (Nubian) plate, west and northwest of the study area. In total, we use data from 55 continuous stations located roughly in the central EARS to form the velocity field (Fig. 1, S1) and strain rate map (Fig. S2) presented in this manuscript. The majority of stations have time series spanning 2017–2022, with some stations containing data as early as 2002.

2.2. InSAR data

We processed ascending C-band imagery from the Sentinel-1a/b satellites, which are part of the European Space Agency's (ESA) Copernicus program. We processed 23 contiguous SAR frames (~250 × 220 km sections) that cover the central EARS and spatially downsampled interferograms to a resolution of approximately 500 m for the entire area, and 20 m for key areas such as Nairobi and Manyara basin. Data are available roughly every 6–12 days. We primarily examined data from 2016 to 2021 and updated some frames with data from late 2014 to late 2022. Descending data was not included because we are focused on a broad survey approach that leverages cloud-based resources rather than modeling and characterizing a specific, known deformation source. Furthermore, line-of-sight (LOS) decomposition has been shown to be problematic when the source deformation is not well understood (Brouwer and Hanssen, 2022), and is better suited for more targeted studies.

2.3. Cloud-based processing

The computational resources required to process and store the input, output, and auxiliary data for the 5 Sentinel-1 SAR paths exceeds the capabilities of most stand-alone computers (requiring more than 100 Tb of storage). Thus, we developed a workflow that leverages cloud computing resources on Amazon Web Service (AWS) for the first phase of processing, which was to produce stacks of co-registered single look complex (SLC) images and geometry files. Most of the Sentinel-1a/b archive is hosted on AWS servers which allows for easy transfer of data files to the computing resources. Costs of these services are ever-decreasing and can currently be accomplished with total costs on the order of a few thousands of dollars. The primary disadvantage of this type of workflow is that all of the processing decisions must be thoroughly planned before sending large, multi-step jobs to the cloud. It is often the case that parameters need to be adjusted throughout the processing stages, and some steps may need iterations due to unforeseen errors or unplanned circumstances/needs. Processing small batches of data on a local machine allows such flexibility that is not realistic in a cloud-based framework. The steps we took to produce a stack of co-registered SLCs and geometry files are shown in Fig. S2 and are described as follows. See supporting materials section 1 for more details on the cloud-based data processing approach.

2.4. Local time series processing

Much of the study region, excluding arid regions like the Turkana depression, is covered by agricultural fields, forests, savannas, and otherwise vegetated regions. These land cover types tend to have relatively poor coherence when compared with arid/semi-arid regions and rocky land cover types, where InSAR is commonly, and most successfully applied. Poor coherence can result in phase unwrapping errors and often

requires masking out large portions of the interferograms when processed using standard techniques. The persistent scatterer method (e.g., Ferretti et al., 2001) relies on the dominance of individual point scatterer targets within a pixel that tend not to decorrelate with time, and it is commonly used in developed/urban areas. Such scatterers might be stable points like roads or buildings to act as constant reflectors. Similarly, the distributed scatter method (e.g., Lanari et al., 2004) leverages stable scattering characteristics by putting greater weight on more stable pixels but relaxes constraints on pixel selection and makes use of pixels that have short-term coherent behavior. This latter technique tends to work well for natural terrain, where scatterers are more distributed like in the majority of our EARS study area (e.g., Hooper, 2008). Thus, we implemented a distributed scatterer-like approach that estimates spatial and temporal phase stability from the stack of full resolution SLC images, and use that information to weight each pixel when downlooking interferograms (e.g., Murray and Lohman, 2018).

A bias occurs as a result of the non-linearity involved in spatial averaging and filtering in the complex domain and becomes more pronounced in longer time series, as well as with heavier spatial averaging – both of which are characteristics of our dataset (Fig. S3). These biases are known as 'phase-closure biases' (e.g., Ansari et al., 2021; Maghsoudi et al., 2022; Zheng et al., 2022). They can be significantly mitigated by not relying solely on interferograms spanning the shortest time ranges (sequential pairs). In our case we compared two interferometric networks. The first was using only sequential pairs, and the second was using redundant sets of interferograms composed of pairs of the nearest five dates for each SLC. For example, given dates (1, 2, 3) the sequential pairs would be (1–2 and 2–3), and the first redundant pair would be pair (1–3). Using redundant pairs (rather than only sequential pairs) greatly helped to limit the effects of phase-closure and reduced spatial variability by up to 3 cm/yr in the rate map (Fig. S3).

After we assessed the phase stability of the images and formed downsampled interferograms, we estimated their coherence and applied a low-pass spatial filter (Goldstein and Werner, 1998) to remove the very high frequency noise in order to reduce unwrapping errors. Phase unwrapping was done with SNAPHU (Statistical-cost, Network-flow Algorithm for Phase Unwrapping) (Chen and Zebker, 2002). Next, we inverted the stack of redundant interferograms to estimate the displacement time series. Each interferogram was referenced to a manually chosen pixel in an area that has high coherence and no clear deformation signal. We removed a planar function from each interferogram to account for any pervasive long wavelength patterns. We used a combination of metrics to mask low quality data in the time series. This includes average coherence (>0.7), coherence variance (<0.05), and the phase stability estimates from the SLC images (>0.6) (Fig. S5). We also masked pixels that were not consistently connected components after

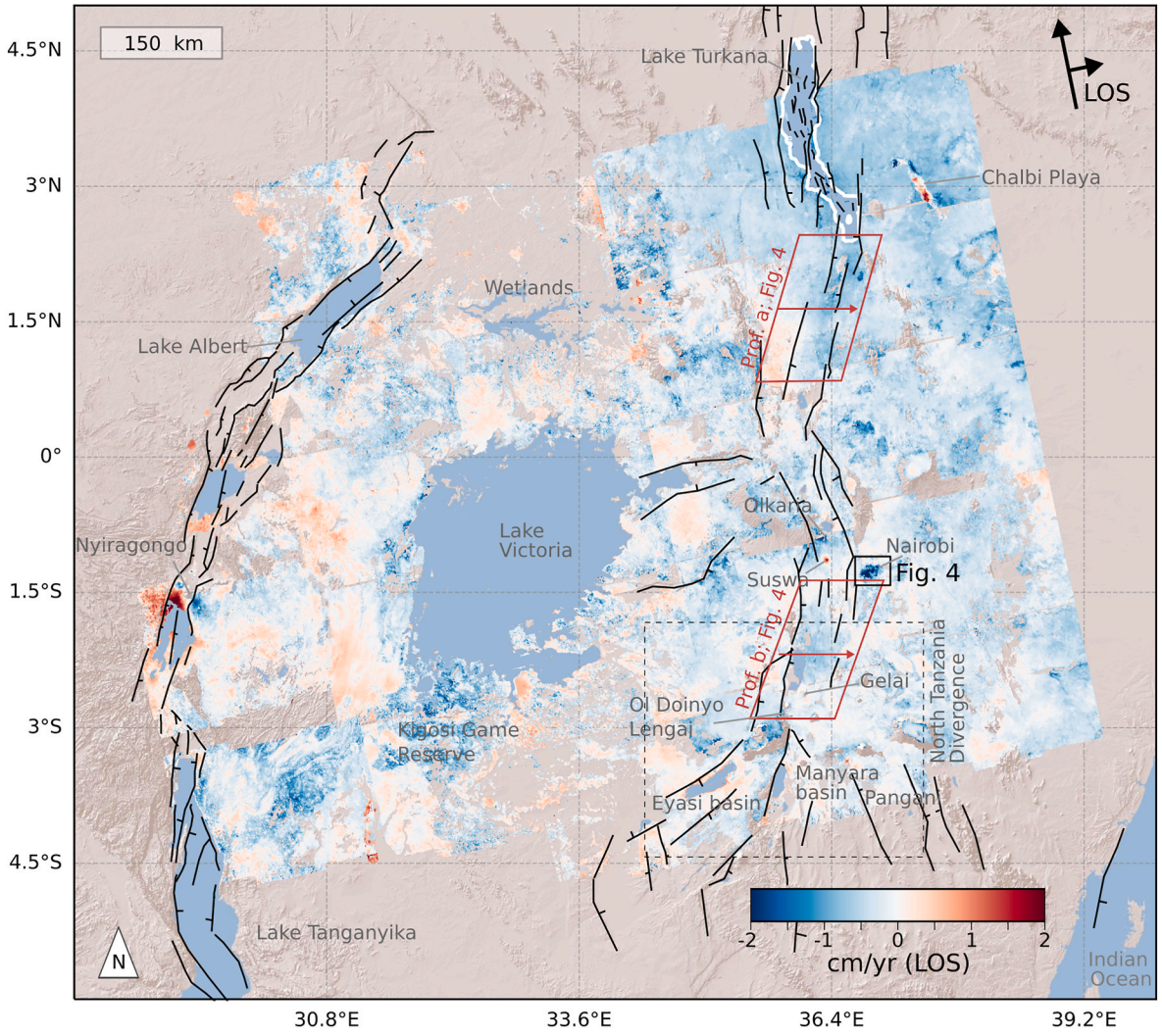

Fig. 2. Ascending Sentinel-1 Line-of-sight (LOS) rate map in Nubia-fixed reference frame. Negative values (blue) represent relative motion away from the satellite (subsidence and/or eastward motion), while positive values (red) represent motion toward the satellite (uplift and/or westward). Major Quaternary faults in black (Ebinger et al., 2024). Lake Turkana outlined in white for clarity.

unwrapping.

Finally, we computed the average LOS displacement rate at each pixel by finding the best linear least squares fit to the displacement time series. The number of SLC images in each stack varies, with 125 on average, and an average of 625 interferograms were used for each stack. To form the complete displacement rate map, we referenced each frame's displacement rate to an average of the intersecting GNSS velocities where available, or to the overlapping InSAR frames in the cases where there were no reliable GNSS velocities within a given frame (Fig. 2).

3. Results

3.1. Tectonic deformation

There is a slight decrease in LOS rate from west to east, relative to stable Nubia. This corresponds to motion away from the satellite which is interpreted as increased eastward motion. Averaging a 100-pixel-wide cross-section across the Kenya Rift south of Lake Turkana results in approximately 4–5 mm/yr of LOS change over a distance of approximately 200 km (Fig. 4a). If we assume this is a result of horizontal motion alone, this equates to approximately 5–6.5 mm/yr which is roughly in agreement with rates derived from GNSS in previous studies (e.g., Knappe et al., 2020). Farther south across the Magadi-Natron basin (Fig. 4b), similarly averaged profiles (also 100-pixels wide) indicate 2–3 mm/yr of LOS change across the rift.

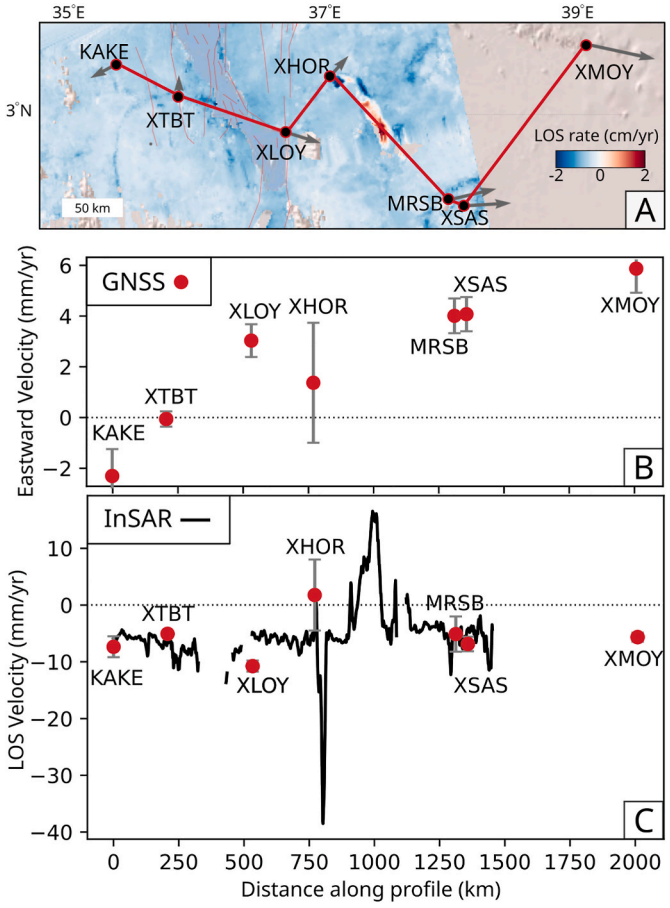

Fig. 3. Profile across the Lake Turkana Depression including Lake Turkana (blue) connecting GNSS stations (King et al., 2019; Knappe et al., 2020). (A) Map showing LOS displacement rates with the GNSS velocity vectors (gray) and profile line (red). Extent of map (A) is shown in Fig. 2. (B) Profile with only the eastward component of the GNSS velocities. (C) GNSS velocities from the profile projected to the InSAR LOS, along with the InSAR LOS rate profile (black line). GNSS uncertainties were computed using the MIDAS method which computes a realistic velocity uncertainty that is based on the observed distribution of sampled slopes (Blewitt et al., 2016). Station XHOR is located at an oasis fed by springs along the margin of a Mesozoic rift system.

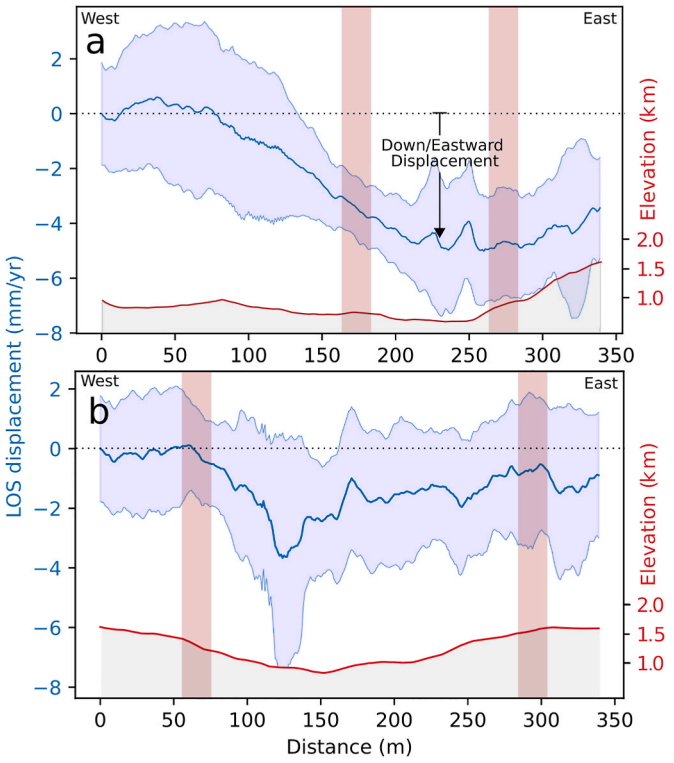

Fig. 4. Averaged profiles of LOS displacements (blue line) with blue shaded region showing standard deviation of measurements, and elevation (red line) along the same profile. Profile spans the eastern branch and locations (a and b) are shown in red box in Fig. 2. Vertical red bars show averaged location of major bounding Quaternary faults.

3.2. Volcanic and magmatic deformation

Our study area exhibits deformation related to volcanic processes at several locations, including Nyiragongo (Smittarello et al., 2022) (Fig. 5) and Suswa (Fig. 6) volcanoes, and a previously unidentified uplift near the Monduli and Meru volcanoes, situated east of the Manyara rift basin.

At Nyiragongo volcano, as depicted in Fig. 5, we identified a clear deformation pattern that aligns with what is typically expected from a dike intrusion. It is characterized by a displacement of approximately +70 cm in LOS on the western lobe (LOS shortening) and approximately −30 cm LOS displacement on the eastern lobe (LOS lengthening). This confirms previous work (e.g., Smittarello et al., 2022).

We do not observe any definitive deformation signals over this time period or at any other time between 2016 and 2022 at Oldoinyo Lengai or the nearby Gelai volcano, both of which are seismically active (e.g., Reiss et al., 2022). However, we do observe a pronounced uplift signal with a spatial extent of ~6 km located on the southern flanks of Monduli and Meru volcanoes, and between Arusha and the rapidly growing town of Kisongo in Tanzania centered at (36.574°E, 3.371°S) (Fig. 7). LOS displacement of the observed signal is sustained at a constant average rate of 2.8 cm/yr over the six-year period of observations (2016–2022). Assuming this is primarily vertical, this equates to approximately 3.6 cm/yr of uplift.

Deflation of Suswa volcano was documented between 1997 and 2000 (Biggs et al., 2009), and ongoing inflation was documented in 2018–2019 (Albino and Biggs, 2021). We have found the inflation event

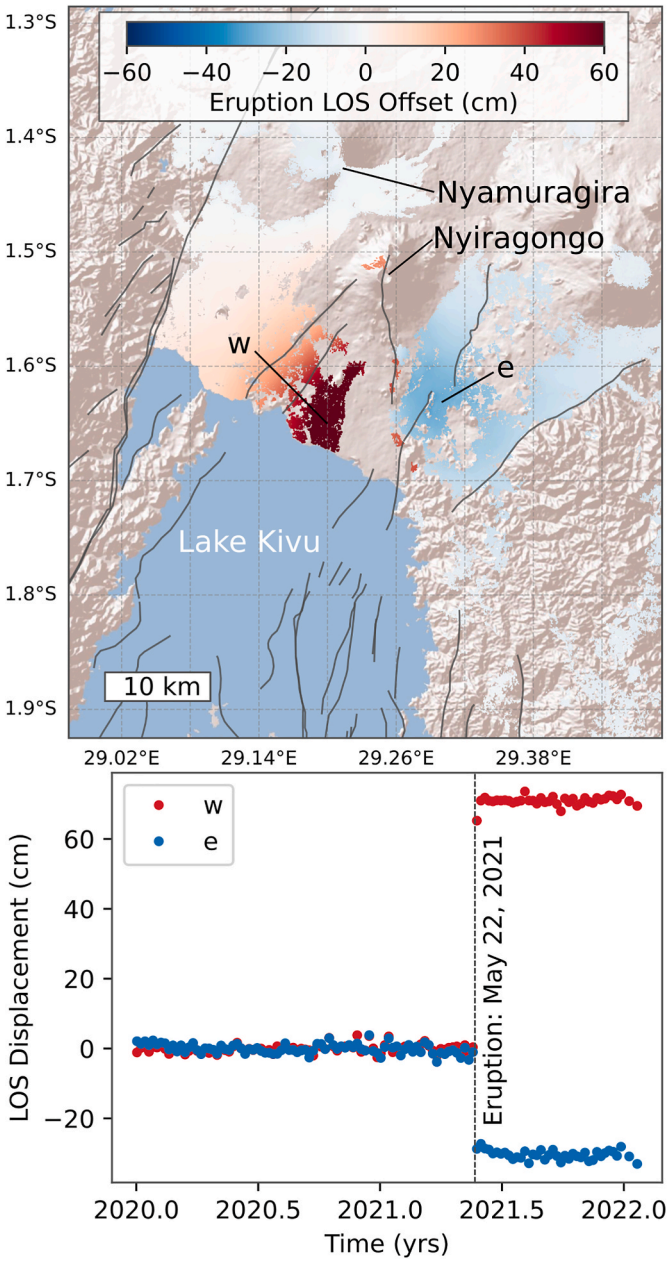

Fig. 5. (A) Map of LOS displacements for 2021 spanning the May 22 eruption of Nyiragongo volcano with fault lines in dark gray (Wood et al., 2017). Map extent shown in Fig. 2. (B) Time series from points w and e (locations in A) which are centered on the two deformation lobes from the dike intrusion.

ceased in late 2019 and we observed no activity up to the end of our observation period in mid-2022 (Fig. 6).

3.3. Hydrologic and anthropogenic deformation

Albino and Biggs (2021) documented sustained subsidence of ~2.5 cm/yr from 2015 to 2020 with Sentinel-1 data at the Olkaria geothermal fields located in the Kenyan Rift. We have extended this observation with three more years of data and have found subsidence has continued at a similar rate (Fig. 8). Displacement rates tend to be quite linear across the geothermal production area with little variation between the main subsidence cones (Fig. 8).

We observe significant wide-spread subsidence across Nairobi related to groundwater extraction from 2015 to 2023. The maximum subsidence occurs in the western part of the city in a predominately

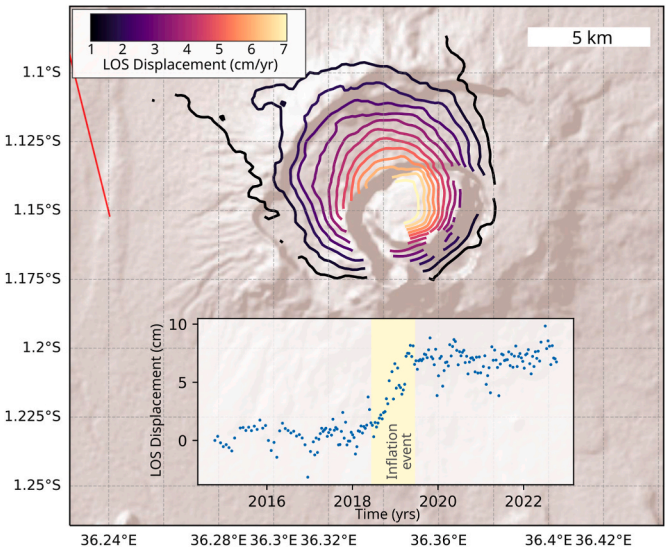

Fig. 6. Uplift at Mount Suswa. Each contour indicates approximately 0.5 cm/yr of LOS motion toward the satellite during the period highlighted in yellow in the time series. Map extent shown in Fig. 2.

residential area (labeled 1 in Fig. 9). Maximum rates are ~6 cm/yr LOS in this area (8.5 cm/yr assuming subsidence). Other localized areas of subsidence are observed with similar rates moving east and north. For example, in the location of GNSS station RCMN (See white triangle in Fig. 9), which is in the farthest northeast of the observed signals, subsidence begins in 2019 with a similar rate to the area of sustained subsidence in the west.

4. Discussion

4.1. Noise

Although areas of poor interferometric coherence are masked with strict criteria, noise still remains present in many areas of the final deformation products, necessitating careful interpretation. Noise found in the LOS rate estimates results primarily from heterogeneous surface properties and processes such as spatial and temporal variation in vegetation and soil moisture. For example, the area directly to the southwest of Lake Victoria hosts very heterogeneous land cover–predominantly a mix of forests and agricultural fields which are notoriously noisy as a result of growing and harvesting crops, tilling fields, and from soil moisture variations that result from irrigation or rainfall (e.g., Jiang and Lohman, 2021). Even farther to the southwest, a clear discontinuity is visible where the land cover changes from mixed agriculture to a state preserved vegetated/forested area known as the Kigosi Game Reserve where there is no farming (Fig. 2, S4). In this example, it is possible that some of the agricultural areas (See Fig. S9 for land cover map) southwest of Lake Victoria show real deformation (e.g., land subsidence from groundwater extraction for irrigation). However, the signal-to-noise level is too low to make meaningful interpretations. 2-sigma uncertainties for the average rate estimations lie generally within 0.5 cm/yr (Fig. S6), but this is likely an underestimate of the true uncertainties due to temporal correlations in the time series. Additionally, it is difficult to accurately propagate uncertainties throughout the various processing stages, like phase unwrapping, that add non-linear characteristics. An alternative approach to cumulative uncertainty estimation is to compare with GNSS-determined velocities. Comparisons with GNSS-derived velocities show InSAR LOS values deviate within a 2-sigma range of 1.04 cm/yr from the GNSS-derived values (Figs. S7 and S8). This range is affected by both noise in the InSAR data as well as noise within the GNSS measurements, which tends to be elevated in the

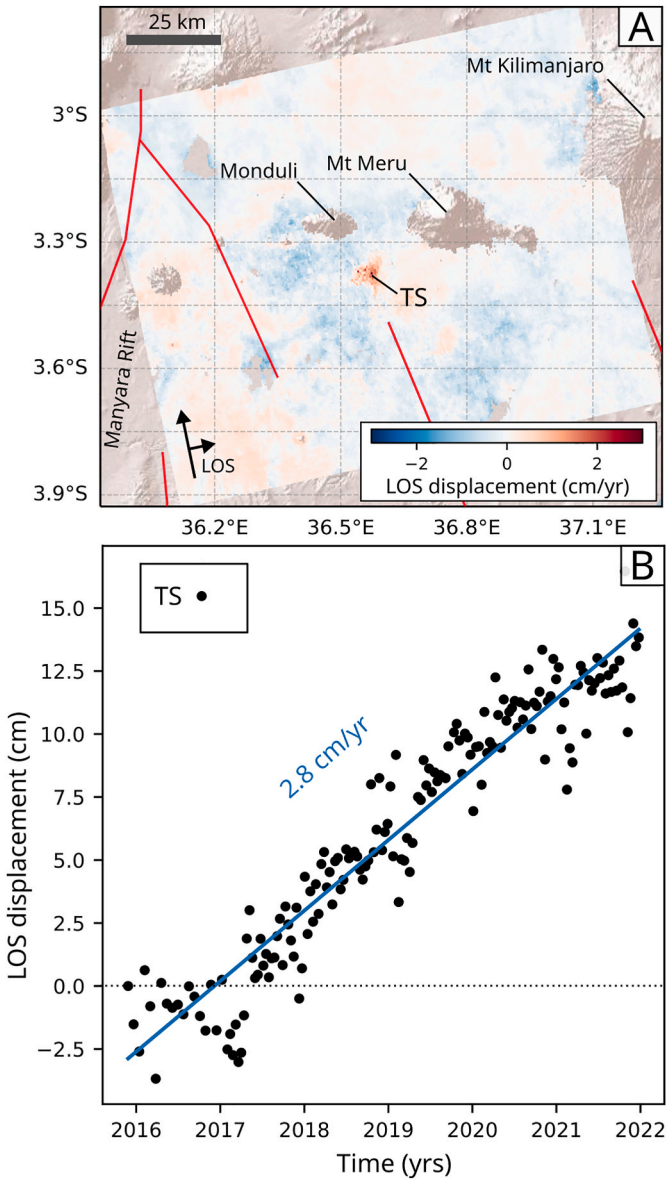

Fig. 7. Uplift signal in the Manyara basin near Mt. Meru with a steady trend since 2016. Time series (B) from point labeled 'TS' on LOS rate map (A). Map extent shown in Fig. 2.

vertical component. Thus, the 2-sigma rate uncertainties of 0.5 cm/yr and the 2-sigma deviations from GNSS-derived displacements of 1.04 cm/yr can be viewed generally as lower- and upper-range estimates of the true uncertainty. Below we present examples only of signals that rise above 1 cm/yr for individual pixels. Note, differential values reported across the Kenya Rift in the following section are below 1 cm/yr, but they are derived from averaging hundreds of pixels. The standard error of the mean scales by $1/\sqrt{n}$, where n is the number of pixels being averaged.

4.2. Tectonics

The analysis of average line-of-sight (LOS) rates over the period from 2016 to 2022 offers valuable insights into the regional deformation trends and highlights potential variations between the Western and Eastern rift zones of the East African Rift System (EARS), as well as along their respective lengths. This analysis is visually represented in Fig. 2.

Present-day rift opening velocities in the EARS are poorly constrained, particularly south of the Main Ethiopian Rift. Strain rates estimated from GNSS data suggest higher rates in the Eastern rift than the Western rift (Fig. S2), consistent with our large-scale observations (Fig. 2). However, the strain rate field (derived from GNSS data) is limited to where there are reliable GNSS stations, thus the results for areas with few or no stations are not conclusive. The sparse network of GNSS stations that are available, along with rigid-plate tectonic models, suggest opening velocities ranging from approximately 2 to 6 mm/year. This estimation presupposes an absence of deformation west of the Western rift and in the offshore regions of Africa (e.g., Doubre et al., 2017; Knappe et al., 2020). This velocity range falls approximately within the noise level typically associated with displacement rates measured by InSAR LOS. This presents a significant challenge in accurately measuring and confidently interpreting long-term tectonic motion in this area.

We observed a lack of significant tectonic strain to the west of Lake Turkana, and more broadly, in the regions west of the eastern branch of the East African Rift System. This finding is particularly noteworthy in light of the data gaps in Southern Sudan, an area that experienced four earthquakes with magnitudes greater than six in 1990. These earthquakes suggest a potential geological connection between the Western Rift and the Main Ethiopian Rift north of our study area, as proposed by Musila et al. (2023). However, it is important to acknowledge the challenges in acquiring reliable InSAR data in the Western Rift regions, where dense vegetation and forest cover can impede accurate measurements. Despite these limitations, our observations, combined with the sparse coverage of the GNSS network, indicate that the extension of the rift is predominantly occurring in the eastern areas, particularly near the Turkana depression. This conclusion aligns with findings from previous research (Ebinger et al., 2000; Vetel and Le Gall, 2006; Knappe et al., 2020), which also support the predominance of rift activity in the eastern branches affected by more voluminous magmatism. Our data supports that the Lake Turkana area, which occupies a narrow part of the broad depression, is likely a major focus area for extensional strain accommodation, and that only a small part of the broad depression is currently deforming. This is thought to be a consequence of eastward strain migration and strain narrowing related to its relatively low elevation/topography and thin crust (e.g., Knappe et al., 2020; Ogden et al., 2022; Musila et al., 2023). This may also be a consequence of focusing of deformation in relation to direct linkage between the Ethiopian and Kenyan rifts (Corti et al., 2019).

In the Eastern Rift, an analysis of a profile line connecting GNSS stations in the southern Turkana region reveals a notable increase in eastward velocities when traversing the rift from west to east, as illustrated in Fig. 3a. After projecting the GNSS velocities onto the InSAR LOS vector, we see reasonable agreement between the two datasets. However, there is more noise present due to the sensitivity of the LOS vector to vertical displacements (Fig. 3c). Displacements that are not generally in the east-west direction are unlikely to be tectonic. This underscores the need for careful interpretation of 1-dimensional InSAR measurements and the need for 2 or more deformation components, including the descending tracks, in future studies that focus on horizontal tectonic motion. Fig. 3 presents a compelling case study of the potential for non-tectonic influences on GNSS sites. The GNSS station XHOR, located in and near the dry lake beds of the Chalbi playa – the heart of an inland drainage basin – shows considerable displacement rates. These rates, as clearly highlighted in the InSAR velocity field (3), are likely associated with the dynamics of the shallow groundwater system in the region (Nyamweru, 1986). This observation provides an example of how local factors can impact GNSS measurements, necessitating careful analysis to distinguish between tectonic movements and other geological or hydrologic processes.

4.2.1. Nyiragongo

Mount Nyiragongo is located in a seismically and volcanically active sector of the Western rift along the ~200 km-wide deforming zone between the Nubian (west) and the small Victoria microplate to the east

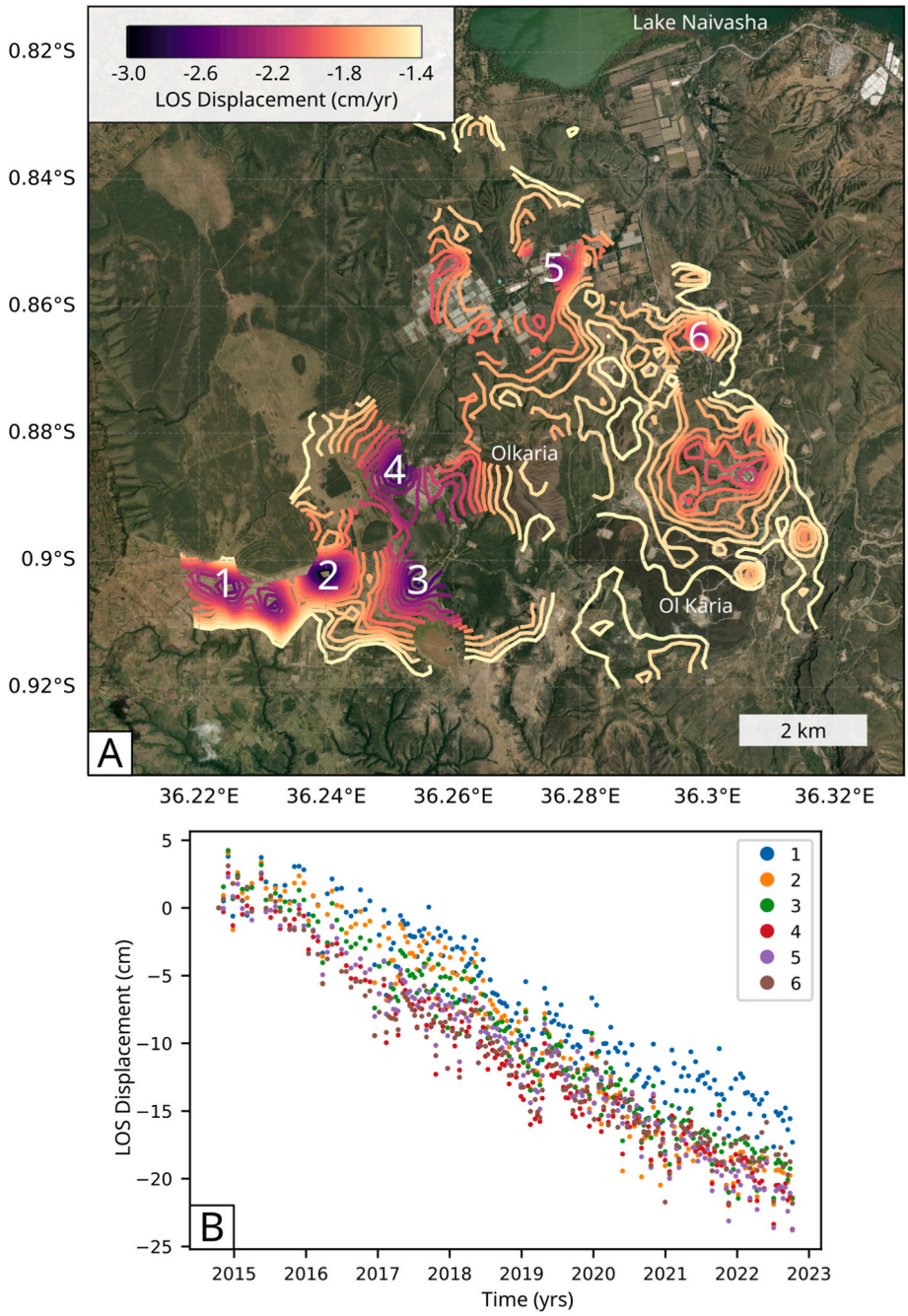

Fig. 8. Sustained subsidence at the Olkaria geothermal plant. (A) LOS displacement rates. Each contour represents ~1 mm/yr. Colors in time series (B) correspond to numbers 1–6 labeled in map (A). Map extent shown in Fig. 2.

(1). It lies just north of Goma, DRC, and Rubavu, Rwanda which together host at least 1.6 million people. The rapid city growth and encroachment up the volcanic slopes makes this population and surrounding communities highly vulnerable to extrusive and intrusive magmatism (e.g., Michellier et al. (2020); Nyiragongo's 2002 eruption was one of the most destructive in the volcano's history, resulting in the loss of at least 150 lives and the displacement of tens of thousands of people (Tedesco et al., 2007; Boudoire et al., 2022). The most recent eruption started on May 22, 2021 and also resulted in the loss of at least 32 lives and thousands of people displaced from their homes in both Rwanda and DRC (e.g., Boudoire et al., 2022). Nyiragongo is characterized by more constant strombolian-type activity with an active lava lake at its crater. Smittarello et al. (2022) reported no clear precursors to the eruption using time series of GNSS measurements and seismicity. Rather, they found an initial rupture of the edifice followed by magma movement and dike intrusion. Here we add to their results with the full time history of the eruption leading to, and directly after the eruption (Fig. 5b).

4.2.2. *North Tanzania divergence*

The Eastern rift diverges into three rift arms in northern Tanzania (Fig. 2) where the western arm transects the Archean craton (Eyasi basin). The Manyara Basin is the central arm, and a poorly defined fault zone to the east, the Pangani Trough, marks the third arm (e.g., Muirhead et al., 2015). The three rift arms are linked by a broad chain of volcanoes that trend younger to the east, although much of the chain is active or dormant. This includes Oldoinyo Lengai, which erupted most recently in 2019, as well as hundreds of undated monogenetic cones. Although we did not observe volcanic-related deformation of Oldoinyo

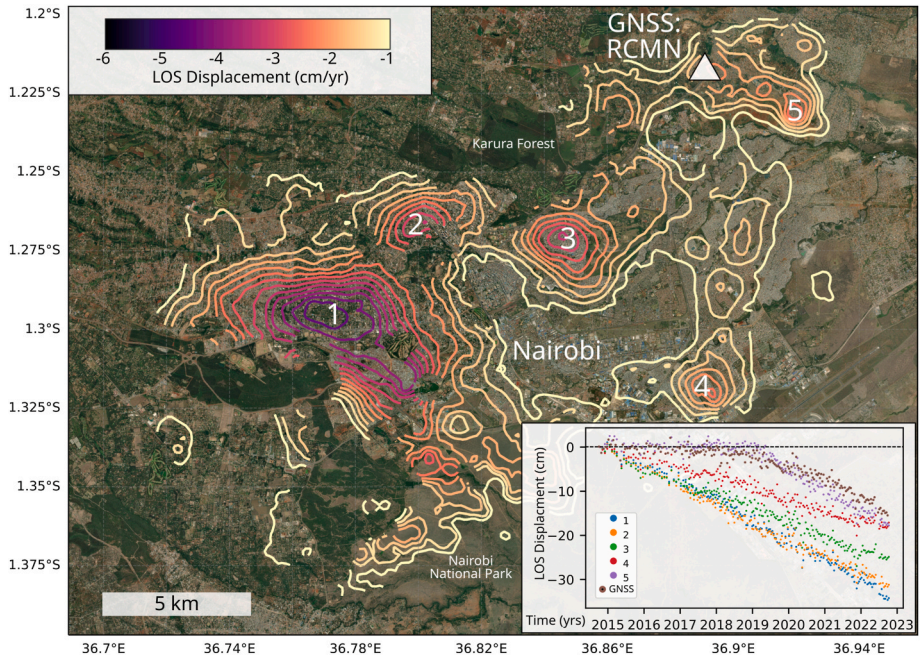

Fig. 9. Average LOS rates related to groundwater extraction in and around Nairobi, Kenya. Each contour represents ~33 mm/yr of LOS change. The GNSS station RCMN is shown as a white triangle on the map and projected to the InSAR LOS for comparison in the inset time series. Colors in time series (inset) correspond to numbers 1–5 labeled in map. Map extent shown in Fig. 2.

Lengai specifically, more targeted studies using higher resolution may illuminate smaller-scale features not resolved in our survey such as for Oldoinyo Lengai (e.g., Daud et al., 2023).

Although the source of this signal remains unclear, and no subsurface data exists in this area (Fig. 7), it may be a result of shallow magmatic activity, given the context of active volcanism and high density of young (< 0.5 ma) monogenetic volcanoes in the surrounding area (Muirhead et al., 2015; Mana et al., 2015; Delcamp et al., 2019). These are generally sourced from dike and sill intrusions which are dictated by the regional and local stress fields from magmatism, as well as mechanical interactions between rift segments (Muirhead et al., 2015; Oliva et al., 2019). Muirhead et al. (2015) proposed that the radial patterns found on these small cones are likely caused by local stress fields induced by shallow magma chambers beneath the volcanic centers, based on the overlapping ages of the cones and the volcanic edifices (Sherrod et al., 2013; Mana et al., 2015). Seismic surveys just to the northwest (Oliva et al., 2019; Reiss et al., 2022) illuminated active hydrothermal systems in shallow connected fracture zones, but did not observe any obvious synchronous seismicity co-located with the observed signal. However, seismic stations in these studies were focused on the Natron basin and did not extend south of Meru and Monduli. It should also be noted that there is a sub N-S striking fault with clear surface expression less than 10 km south of the uplifting zone which appears to be on the footwall of the fault. Northward propagation of the fault zone cannot be ruled out as a possible source.

4.2.3. Mount Suswa

Mount Suswa is a Quaternary volcano located in the southern Kenya Rift. The most recent volcanism occurred less than 1000 years ago, but no eruptions have occurred in recorded history (Simiyu, 2010). In recent years, Suswa Volcano has been a site of geothermal exploration, as it is thought to have significant shallow magmatic activity (Simiyu, 2010). Our updated observations now bracket deformation at Suswa volcano, providing a reference for the rate and magnitude of the transient inflation event.

4.2.4. Olkaria

The Olkaria geothermal field is located just north of Mount Suswa in the Kenyan Rift Valley, near the town of Naivasha. It is one of the largest and most active geothermal fields in Africa, and it is a major source of geothermal energy for Kenya, operating since 1981 (Simiyu, 2010; Mangi, 2018). Given the sustained linear rates we observe, geothermal energy production is inducing a steady subsidence rate that may eventually have consequences for groundwater and induced seismicity.

4.2.5. Nairobi

Nairobi, Kenya is a large urban area with a metropolitan population of over 10 million people. It relies heavily on groundwater resources for domestic, agricultural, and industrial purposes, and groundwater usage has seen exponential acceleration since the mid-1970's keeping pace with population growth (Foster et al., 2018; Oiro et al., 2020). Groundwater is typically found in volcano-sedimentary aquifers, and an increasing number of boreholes are being drilled to meet demand. This has been accentuated in recent years by worsening drought conditions in the area and has led to over-extraction of regional aquifers (Oiro et al., 2020). Over-extraction of groundwater leads to decreased pore water pressure in aquifers and will ultimately result in depletion. The decrease in pore water pressure leads to an increase in the effective lithostatic stress in the shallow crust, which causes subsidence of the surface above it (e.g., Poland and Davis, 1969). However, in the areas farther northeast, subsidence begins later. This suggests, as groundwater pumping continues, subsidence rates are sustained across the metro area, but the spatial extent is extending over time – predominantly towards the north east.

5. Conclusions

We conducted a broad, satellite-based, geodetic survey of the central EARS in order to identify new signals and establish a baseline for tectonic, volcanic, and anthropogenic change. We have also demonstrated a new regional InSAR processing flow that leverages cloud-computing resources to produce InSAR time series of LOS displacements over a large section of the EARS. This complements sparse local GNSS

measurements spanning a region with extensional velocities less than 6 mm/yr, near the limit of GNSS detection. InSAR data quality is variable due to heterogeneous surface characteristics, making it a challenging area to study deformation with InSAR. However, in more arid areas, regions with less active agricultural activity, and/or in the case of displacements with high signal-to-noise ratios, we have successfully constrained a range of important deformation features. These have implications for the safety and sustainability of the large and rapidly growing populations inhabiting these regions.

Tectonic rates within our study area are generally quite low, making it difficult or impossible to constrain for large parts of the central EARS. However, averaging data, particularly across the Kenya Rift shows a differential rate of approximately 5 mm/yr from west to east across a zone of 100 km or less near Lake Turkana, and 2–3 mm/yr farther south near the Natron Basin.

There has been active volcanic deformation in several areas within the study region since our measurements begin in 2015. We presented displacements from volcanic activity from the 2021 eruption of Nyiragongo volcano of ~70 cm LOS maximum offset on the western lobe and −30 cm LOS maximum offset on the eastern lobe. We presented measurements of an inflation event at the summit of Mount Suswa occurring from mid-2018 to mid-2019. This resulted in ~7 cm LOS displacement (9 cm assuming uplift), but it has remained stable up to the end of 2022. We found a sustained displacement signal located south of Monduli and Meru volcanoes, west of Arusha, Tanzania with sustained rates of 2.8 cm/yr (3.6 cm/yr assuming the signal is predominately uplift). Given the context of active volcanism and young cinder cones in the vicinity, this may be related to magmatic and/or hydrothermal activity, but requires additional ground-truthing.

Population growth and industrial development is beginning to also leave a deformation signature in some areas in the region. This comes in the form of subsidence from both groundwater extraction and geothermal production. Extensive groundwater extraction in Nairobi, Kenya is resulting in up to −6 cm/yr of LOS displacement (~-8 cm/yr assuming only subsidence). Areas of subsidence appear to be extending from western Nairobi eastward as groundwater pumping continues to tax regional aquifers. Finally, we presented measurements of subsidence resulting from continued geothermal production at the Olkaria geothermal power station in southwestern Kenya. Subsidence rates are constant over the time period of observation with rates up to −3 cm/yr in the LOS (−4 cm/yr assuming all subsidence).

This rich dataset contains measurements of deformation from a wide variety of natural and anthropogenic source processes. This emphasizes the ongoing activity within the EARS and the need to continually study and monitor active deformation in this region. Although this study represents a brief time span and contains gaps due to noise, it is a step towards a more complete picture of deformation in the central EARS. Many signals are present between GNSS stations, and many GNSS stations lie within areas deforming due to non-tectonic processes. This must be considered and/or mitigated when performing studies based on strain fields and Euler-pole models derived from the GNSS network.

CRediT authorship contribution statement

Kyle Dennis Murray: Writing – original draft, Visualization, Validation, Software, Resources, Methodology, Investigation, Funding acquisition, Formal analysis, Data curation, Conceptualization. **Cynthia J. Ebinger:** Writing – review & editing.

Declaration of competing interest

The authors declare that they have no known competing financial interests or personal relationships that could have appeared to influence the work reported in this paper.

Data availability

Data will be shared on an external website

Acknowledgments

Copernicus Sentinel-1 SAR imagery used in this study is from the European Space Agency (ESA), downloaded through the Alaska Satellite Facility (ASF) at https://vertex.daac.asf.alaska.edu. The Jet Propulsion Laboratory freely provides The InSAR Scientific Computing Environment (ISCE) (Rosen et al., 2012), along with the stack processing capability (Fattahi et al., 2016). SRTM topographic data (Farr et al., 2007) were obtained by the United States Geological Survey EROS archive https://www.usgs.gov/centers/eros/science/usgs-eros-archive-digital-elevation-shuttle-radar-topography-mission-srtm-1. GNSS data were obtained from the GeoPRISM's archived velocity field (MIT 2019.0) for the East African Rift System generated by King et al., (2019), as well as the Nevada Geodetic Laboratory (http://geodesy.unr.edu/velocities/midas.AF.txt). Earthquake locations were obtained from https://earthquake.usgs.gov/. Location of volcanic centers were obtained from the Global Volcanism Program (Venzke, 2013).

This project is supported by the NSF GeoPRISMS postdoctoral fellowship (NSF EAR1949073). Cloud processing was funded through AWS research credits through the program https://aws.amazon.com/government-education/research-and-technical-computing/cloud-credit-for-research/. Thank you to Bridget Smith-Konter and Matthew Pritchard for early discussions and feedback on the project and paper. Constructive feedback from editors Read Mapeo and Barb Tewksbury, and two anonymous reviewers improved the manuscript.

Appendix A. Supplementary data

Supplementary data to this article can be found online at https://doi.org/10.1016/j.jafrearsci.2024.105390.

References

Albino, F., Biggs, J., 2021. Magmatic processes in the East african Rift system: insights from a 2015–2020 sentinel-1 InSAR survey. G-cubed 22, e2020GC009488.

Ansari, H., De Zan, F., Parizzi, A., 2021. Study of systematic bias in measuring surface deformation with SAR interferometry. IEEE Trans. Geosci. Rem. Sens. 59, 1285–1301. https://doi.org/10.1109/TGRS.2020.3003421.

Baer, G., Hamiel, Y., Shamir, G., Nof, R., 2008. Evolution of a magma-driven earthquake swarm and triggering of the nearby oldoinyo lengai eruption, as resolved by insar, ground observations and elastic modeling, east african rift, 2007. Earth Planet Sci. Lett. 272, 339–352.

Bendick, R., McClusky, S., Bilham, R., Asfaw, L., Klemperer, S., 2006. Distributed Nubia—Somalia relative motion and dike intrusion in the Main Ethiopian Rift. Geophys. J. Int. 165, 303–310.

Biggs, J., Anthony, E.Y., Ebinger, C.J., 2009. Multiple inflation and deflation events at Kenyan volcanoes, East African Rift. Geology 37, 979–982. https://doi.org/10.1130/G30133A.1.

Bilham, R., Bendick, R., Larson, K., Mohr, P., Braun, J., Tesfaye, S., Asfaw, L., 1999. Secular and tidal strain across the main Ethiopian rift. Geophys. Res. Lett. 26, 2789–2792. https://doi.org/10.1029/1998GL005315.

Birhanu, Y., Bendick, R., Fisseha, S., Lewi, E., Floyd, M., King, R., Reilinger, R., 2016. GPS constraints on broad scale extension in the Ethiopian Highlands and Main Ethiopian Rift. Geophys. Res. Lett. 43, 6844–6851. https://doi.org/10.1002/2016GL069890.

Birhanu, Y., Williams, S., Bendick, R., Fisseha, S., 2018. Time dependence of noise characteristics in continuous GPS observations from East Africa. J. Afr. Earth Sci. 144, 83–89.

Blewitt, G., Kreemer, C., Hammond, W.C., Gazeaux, J., 2016. MIDAS robust trend estimator for accurate GPS station velocities without step detection. J. Geophys. Res. Solid Earth 121, 2054–2068.

Borsa, A.A., Agnew, D.C., Cayan, D.R., 2014. Ongoing drought-induced uplift in the western United States. Science. https://doi.org/10.1126/science.1260279 (New York, N.Y.).

Boudoire, G., Calabrese, S., Colacicco, A., Sordini, P., Habakaramo Macumu, P., Rafflin, V., Valade, S., Mweze, T., Kazadi Mwepu, J.C., Safari Habari, F., Amani Kahamire, T., Mumbere Mutima, Y., Ngaruye, J.C., Tuyishime, A., Tumaini Sadiki, A., Mavonga Tuluka, G., Mapendano Yalire, M., Kets, E.D., Grassa, F., D'Alessandro, W., Caliro, S., Rufino, F., Tedesco, D., 2022. Scientific response to the 2021 eruption of Nyiragongo based on the implementation of a participatory

monitoring system. Sci. Rep. 12, 7488. https://doi.org/10.1038/s41598-022-11149-0.
Boyce, A., Kounoudis, R., Bastow, I., Cottaar, S., Ebinger, C., Ogden, C., 2023. Mantle Wavespeed and Discontinuity Structure below East Africa: Implications for Cenozoic Hotspot Tectonism and the Development of the Turkana Depression.
Brouwer, W.S., Hanssen, R., 2022. A treatise on insar geometry and 3d displacement estimation. IEEE Trans. Geosci. Rem. Sens. 61, 1–11.
Chen, C.W., Zebker, H.A., 2002. Phase unwrapping for large SAR interferograms: statistical segmentation and generalized network models. IEEE Trans. Geosci. Rem. Sens. 40, 1709–1719. https://doi.org/10.1109/TGRS.2002.802453.
Corti, G., Cioni, R., Franceschini, Z., Sani, F., Scaillet, S., Molin, P., Isola, I., Mazzarini, F., Brune, S., Keir, D., et al., 2019. Aborted propagation of the ethiopian rift caused by linkage with the kenyan rift. Nat. Commun. 10, 1309.
Daud, N., Stamps, D.S., Battaglia, M., Huang, M.H., Saria, E., Ji, K.H., 2023. Elucidating the magma plumbing system of ol doinyo lengai (natron rift, Tanzania) using satellite geodesy and numerical modeling. J. Volcanol. Geoth. Res. 438, 107821.
Delcamp, A., Mossoux, S., Belkus, H., Tweheyo, C., Mattsson, H.B., Kervyn, M., 2019. Control of the stress field and rift structures on the distribution and morphology of explosive volcanic craters in the Manyara and Albertine rifts. J. Afr. Earth Sci. 150, 566–583. https://doi.org/10.1016/j.jafrearsci.2018.09.012.
Doubre, C., Déprez, A., Masson, F., Socquet, A., Lewi, E., Grandin, R., Nercessian, A., Ulrich, P., De Chabalier, J.B., Saad, I., Abayazid, A., Peltzer, G., Delorme, A., Calais, E., Wright, T., 2017. Current deformation in Central Afar and triple junction kinematics deduced from GPS and InSAR measurements. Geophys. J. Int. 208, 936–953. https://doi.org/10.1093/gji/ggw434.
Doubre, C., Peltzer, G., 2007. Fluid-controlled faulting process in the Asal Rift, Djibouti, from 8 yr of radar interferometry observations. Geology 35, 69–72. https://doi.org/10.1130/G23022A.1.
Ebinger, C., Reiss, M.C., Bastow, I., Karanja, M.M., 2024. Shallow sources of upper mantle seismic anisotropy in east africa. Earth Planet Sci. Lett. 625, 118488.
Ebinger, C.J., Casey, M., 2001. Continental breakup in magmatic provinces: an Ethiopian example. Geology 29, 527–530. https://doi.org/10.1130/0091-7613.
Ebinger, C.J., Yemane, T., Harding, D.J., Tesfaye, S., Kelley, S., Rex, D., 2000. Rift deflection, migration, and propagation: linkage of the Ethiopian and Eastern rifts, Africa. GSA Bulletin 112, 163–176.
Farr, T.G., Rosen, P.A., Caro, E., Crippen, R., Duren, R., Hensley, S., Kobrick, M., Paller, M., Rodriguez, E., Roth, L., others, 2007. The shuttle radar topography mission. Rev. Geophys. 45.
Fattahi, H., Agram, P., Simons, M., 2016. A network-based enhanced spectral diversity approach for TOPS time-series analysis. IEEE Trans. Geosci. Rem. Sens. 55, 777–786.
Ferretti, A., Prati, C., Rocca, F., 2001. Permanent scatterers in SAR interferometry. IEEE Trans. Geosci. Rem. Sens. 39, 8–20.
Fishwick, S., Bastow, I.D., 2011. Towards a Better Understanding of African Topography: a Review of Passive-Source Seismic Studies of the African Crust and Upper Mantle, vol. 357. Geological Society, London, Special Publications, pp. 343–371. https://doi.org/10.1144/SP357.19.
Foster, S., Bousquet, A., Furey, S., 2018. Urban groundwater use in Tropical Africa – a key factor in enhancing water security? Water Pol. 20, 982–994. https://doi.org/10.2166/wp.2018.056.
Gaherty, J.B., Zheng, W., Shillington, D.J., Pritchard, M.E., Henderson, S.T., Chindandali, P.R.N., Mdala, H., Shuler, A., Lindsey, N., Oliva, S.J., Nooner, S., Scholz, C.A., Schaff, D., Ekström, G., Nettles, M., 2019. Faulting processes during early-stage rifting: seismic and geodetic analysis of the 2009–2010 Northern Malawi earthquake sequence. Geophys. J. Int. 217, 1767–1782. https://doi.org/10.1093/gji/ggz119.
Goldstein, R.M., Werner, C.L., 1998. Radar interferogram filtering for geophysical applications. Geophys. Res. Lett. 25, 4035–4038. https://doi.org/10.1029/1998GL900033.
Hamling, I.J., Wright, T.J., Calais, E., Lewi, E., Fukahata, Y., 2014. InSAR observations of post-rifting deformation around the Dabbahu rift segment, Afar, Ethiopia. Geophys. J. Int. 197, 33–49. https://doi.org/10.1093/gji/ggu003.
Hodge, M., Fagereng, A., Biggs, J., Mdala, H., 2018. Controls on early-rift geometry: new perspectives from the bilila-mtakataka fault, Malawi. Geophys. Res. Lett. 45, 3896–3905. https://doi.org/10.1029/2018GL077343.
Hooper, A., 2008. A multi-temporal insar method incorporating both persistent scatterer and small baseline approaches. Geophys. Res. Lett. 35.
Jiang, J., Lohman, R.B., 2021. Coherence-guided InSAR deformation analysis in the presence of ongoing land surface changes in the Imperial Valley, California. Rem. Sens. Environ. 253, 112160 https://doi.org/10.1016/j.rse.2020.112160.
Johnson, T.C., Kelts, K., Odada, E., 2000. The Holocene history of Lake Victoria. Ambio 29, 2–11.
Jones, J.R., Stamps, D.S., Wauthier, C., Saria, E., Biggs, J., 2019. Evidence for slip on a border fault triggered by magmatic processes in an immature continental rift. G-cubed 20, 2515–2530. https://doi.org/10.1029/2018GC008165.
King, R., Floyd, M., Reilinger, R., Bendick, R., 2019. GPS velocity field (MIT 2019.0) for the East African Rift System generated by King et al.
Knappe, E., Bendick, R., Ebinger, C., Birhanu, Y., Lewi, E., Floyd, M., King, R., Kianji, G., Mariita, N., Temtime, T., Waktola, B., Deresse, B., Musila, M., Kanoti, J., Perry, M., 2020. Accommodation of East African rifting across the turkana depression. J. Geophys. Res. Solid Earth 125, e2019JB018469. https://doi.org/10.1029/2019JB018469.
Lanari, R., Lundgren, P., Manzo, M., Casu, F., 2004. Satellite radar interferometry time series analysis of surface deformation for Los Angeles, California. Geophys. Res. Lett. 31, 1–5. https://doi.org/10.1029/2004GL021294.
Lavayssiere, A., 2019. Interactions between Tectonic and Magmatic Processes in the East African Rift. Phd. University of Southampton.
Maghsoudi, Y., Hooper, A.J., Wright, T.J., Lazecky, M., Ansari, H., 2022. Characterizing and correcting phase biases in short-term, multilooked interferograms. Rem. Sens. Environ. 275, 113022.
Mana, S., Furman, T., Turrin, B.D., Feigenson, M.D., Swisher III, C.C., 2015. Magmatic activity across the East african north Tanzanian divergence zone. J. Geol. Soc. 172, 368–389. https://doi.org/10.1144/jgs2014-072.
Mangi, P.M., 2018. Geothermal development in Kenya- country updates. In: Proceedings, 7th African Rift Geothermal Conference. Kigali, Rwanda.
Mcconnell, R.B., 1967. The East african Rift System. Nature 215, 578–581. https://doi.org/10.1038/215578a0.
Michellier, C., Kervyn, M., Barette, F., Muhindo Syavulisembo, A., Kimanuka, C., Kulimushi Mataboro, S., Hage, F., Wolff, E., Kervyn, F., 2020. Evaluating population vulnerability to volcanic risk in a data scarcity context: the case of Goma city, Virunga volcanic province (DRCongo). Int. J. Disaster Risk Reduc. 45, 101460 https://doi.org/10.1016/j.ijdrr.2019.101460.
Muirhead, J.D., Kattenhorn, S.A., Le Corvec, N., 2015. Varying styles of magmatic strain accommodation across the East African Rift. G-cubed 16, 2775–2795. https://doi.org/10.1002/2015GC005918.
Murray, K.D., Lohman, R.B., 2018. Short-lived pause in Central California subsidence after heavy winter precipitation of 2017. Sci. Adv. 4, eaar8144.
Musila, M., Ebinger, C.J., Bastow, I.D., Sullivan, G., Oliva, S.J., Knappe, E., Perry, M., Kounoudis, R., Ogden, C.S., Bendick, R., Mwangi, S., Mariita, N., Kianji, G., Klein, E., Illsley-Kemp, F., 2023. Active deformation constraints on the nubia-Somalia plate boundary through heterogeneous lithosphere of the turkana depression. G-cubed (in press).
Nyamweru, C., 1986. Quaternary Environments of the Chalbi Basin, Kenya, vol. 25. Geological Society, London, Special Publications, pp. 297–310.
Ogden, C.S.S., Bastow, I.D., Ebinger, C.J., Kounoudis, R., Musila, M., Sullivan, G., Ayele, A., Bendick, R.O., Mariita, N., karegi Kianji, G., 2022. The development of multiple phases of superposed rifting in the turkana depression, East Africa: evidence from HK stacking of teleseismic receiver functions. In: Fall Meeting 2022.
Oiro, S., Comte, J.C., Soulsby, C., MacDonald, A., Mwakamba, C., 2020. Depletion of groundwater resources under rapid urbanisation in Africa: recent and future trends in the Nairobi Aquifer System, Kenya. Hydrogeol. J. 28, 2635–2656. https://doi.org/10.1007/s10040-020-02236-5.
Oliva, S.J., Ebinger, C.J., Wauthier, C., Muirhead, J.D., Roecker, S.W., Rivalta, E., Heimann, S., 2019. Insights into fault-magma interactions in an early-stage continental rift from source mechanisms and correlated volcano-tectonic earthquakes. Geophys. Res. Lett. 46, 2065–2074. https://doi.org/10.1029/2018GL080866.
Poland, J., Davis, G., 1969. Land-surface subsidence due to the withdrawal of fluids. Rev. Eng. Geol. 2, 187–270. https://doi.org/10.1130/REG2-p187.
Reiss, M.C., De Siena, L., Muirhead, J.D., 2022. The interconnected magmatic plumbing system of the natron rift. Geophys. Res. Lett. 49, e2022GL098922 https://doi.org/10.1029/2022GL098922.
Rosen, P.A., Gurrola, E., Sacco, G.F., Zebker, H., 2012. The InSAR scientific computing environment. In: EUSAR 2012; 9th European Conference on Synthetic Aperture Radar, pp. 730–733.
Sherrod, D., Magigita, M., Kwelwa, S., 2013. Geologic Map of Oldonyo Lengai (Oldoinyo Lengai) and Surroundings, Arusha Region, United Republic of Tanzania: U.S. Geological Survey Open-File Report. Open-File Report. United States Geological Survey.
Simiyu, S.M., 2010. Status of geothermal exploration in Kenya and future plans for its development. In: Proceedings World Geothermal Congress 2010. Bali, Indonesia.
Smittarello, D., d'Oreye, N., Jaspard, M., Derauw, D., Samsonov, S., 2022. Pair selection optimization for InSAR time series processing. J. Geophys. Res. Solid Earth 127, e2021JB022825.
Stamps, D., Kreemer, C., Fernandes, R., Rajaonarison, T., Rambolamanana, G., 2021. Redefining East african Rift System kinematics. Geology 49, 150–155. https://doi.org/10.1130/G47985.1.
Stamps, D., Saria, E., Kreemer, C., 2018. A geodetic strain rate model for the East African Rift System. Sci. Rep. 8, 732. https://doi.org/10.1038/s41598-017-19097-w.
Tedesco, D., Vaselli, O., Papale, P., Carn, S.A., Voltaggio, M., Sawyer, G.M., Durieux, J., Kasereka, M., Tassi, F., 2007. 2002 volcano-tectonic eruption of Nyiragongo volcano, Democratic Republic of Congo. J. Geophys. Res. Solid Earth 112. https://doi.org/10.1029/2006JB004762.
Temtime, T., Biggs, J., Lewi, E., Hamling, I., Wright, T., Ayele, A., 2018. Spatial and temporal patterns of deformation at the Tendaho geothermal prospect, Ethiopia. J. Volcanol. Geoth. Res. 357, 56–67. https://doi.org/10.1016/j.jvolgeores.2018.04.004.
Venzke, E.e., 2013. Global volcanism program. Volcanoes of the World 4 (9), 1 (17 Sep 2020).
Vetel, W., Le Gall, B., 2006. Dynamics of Prolonged Continental Extension in Magmatic Rifts: the Turkana Rift Case Study (North Kenya), vol. 259. Geological Society, London, Special Publications, pp. 209–233. https://doi.org/10.1144/GSL.SP.2006.259.01.17.
Wauthier, C., Oyen, A., Marinkovic, P., Cayol, V., Fernandez, Gonzalez, J.P., Hanssen, R., Kervyn, F., d'Oreye, N., Shirzaei, M., Walter, T.R., 2009. L-band and C-band InSAR studies of African volcanic areas. In: 2009 IEEE International Geoscience and Remote Sensing Symposium, pp. II-210–II-213. https://doi.org/10.1109/IGARSS.2009.5418043.
Wauthier, C., Smets, B., Hooper, A., Kervyn, F., d'Oreye, N., 2018. Identification of subsiding areas undergoing significant magmatic carbon dioxide degassing, along the northern shore of Lake Kivu, East African Rift. J. Volcanol. Geoth. Res. 363, 40–49.

Weinstein, A., Oliva, S.J., Ebinger, C.J., Roecker, S., Tiberi, C., Aman, M., Lambert, C., Witkin, E., Albaric, J., Gautier, S., others, 2017. Fault-magma interactions during early continental rifting: seismicity of the M agadi-N atron-Manyara basins, Africa. G-cubed 18, 3662–3686.

Weiss, J.R., Walters, R.J., Morishita, Y., Wright, T.J., Lazecky, M., Wang, H., Hussain, E., Hooper, A.J., Elliott, J.R., Rollins, C., others, 2020. High-resolution surface velocities and strain for Anatolia from Sentinel-1 InSAR and GNSS data. Geophys. Res. Lett. 47, e2020GL087376.

Wood, D.A., Zal, H.J., Scholz, C.A., Ebinger, C.J., Nizere, I., 2017. Evolution of the kivu rift, east africa: interplay among tectonics, sedimentation and magmatism. Basin Res. 29, 175–188.

Wright, T.J., Ebinger, C., Biggs, J., Ayele, A., Yirgu, G., Keir, D., Stork, A., 2006. Magma-maintained rift segmentation at continental rupture in the 2005 Afar dyking episode. Nature 442, 291–294. https://doi.org/10.1038/nature04978.

Zheng, W., Oliva, S.J., Ebinger, C., Pritchard, M.E., 2020. Aseismic deformation during the 2014 M w 5.2 Karonga earthquake, Malawi, from satellite interferometry and earthquake source mechanisms. Geophys. Res. Lett. 47, e2020GL090930.

Zheng, Y., Fattahi, H., Agram, P., Simons, M., Rosen, P., 2022. On closure phase and systematic bias in multilooked SAR interferometry. IEEE Trans. Geosci. Rem. Sens. 60, 1–11.